

Visible-light all-fiber vortex lasers based on mode selective couplers

Chuchu Dong(董楚楚), Jinhai Zou(邹金海), Hongjian Wang(王鸿健), Han Yao(尧涵), Xianglong Zeng(曾祥龙), Yikun Bu(卜轶坤), Zhengqian Luo(罗正钱)

Citation: Chin. Phys. B . 2020, 29(9): 094204 . **doi:** 10.1088/1674-1056/aba278
Journal homepage: http://cpb.iphy.ac.cn; http://iopscience.iop.org/cpb

What follows is a list of articles you may be interested in

Hyperbolic metamaterials for high-efficiency generation of circularly polarized Airy beams

Lin Chen(陈林), Huihui Li(李会会), Weiming Hao(郝玮鸣), Xiang Yin(殷祥), Jian Wang(王健)

Chin. Phys. B . 2020, 29(8): 084210 . **doi:** 10.1088/1674-1056/ab96a1

Extraordinary propagation characteristics of electromagnetic waves in one-dimensional anti-*PT*-symmetric ring optical waveguide network

Jie-Feng Xu(许杰锋), Xiang-Bo Yang(杨湘波), Hao-Han Chen(陈浩瀚), Zhan-Hong Lin(林展鸿)

Chin. Phys. B . 2020, 29(6): 064201 . **doi:** 10.1088/1674-1056/ab8371

Dynamically adjustable asymmetric transmission and polarization conversion for linearly polarized terahertz wave

Tong Li(李彤), Fang-Rong Hu(胡放荣), Yi-Xian Qian(钱义先), Jing Xiao(肖靖), Long-Hui Zhang(张隆辉), Wen-Tao Zhang(张文涛), Jia-Guang Han(韩家广)

Chin. Phys. B . 2020, 29(2): 024203 . **doi:** 10.1088/1674-1056/ab5ef8

Electrically triggered dual-band tunable terahertz metamaterial band-pass filter based on Si_3N_4-VO_2-Si_3N_4 sandwich

Shuai Zhao(赵帅), Fangrong Hu(胡放荣), Xinlong Xu(徐新龙), Mingzhu Jiang(江明珠), Wentao Zhang(张文涛), Shan Yin(银珊), Wenying Jiang(姜文英)

Chin. Phys. B . 2019, 28(5): 054203 . **doi:** 10.1088/1674-1056/28/5/054203

Optical properties of a three-dimensional chiral metamaterial

Juan-Juan Guo(郭娟娟), Mao-Sheng Wang(汪茂胜), Wan-Xia Huang(黄万霞)

Chin. Phys. B . 2017, 26(12): 124211 . **doi:** 10.1088/1674-1056/26/12/124211

Multi-functional vanadium dioxide integrated metamaterial for terahertz wave manipulation*

Jian-Xing Zhao(赵建行)[1], Jian-Lin Song(宋建林)[1], Yao Zhou(周姚)[1], Rui-Long Zhao(赵瑞龙)[1], Yi-Chao Liu(刘艺超)[1], and Jian-Hong Zhou(周见红)[1,2,†]

[1] *School of Photoelectric Engineering, Changchun University of Science and Technology, Changchun* 130022, *China*
[2] *Key Laboratory of Optoelectric Measurement and Optical Information Transmission Technology of Ministry of Education, Changchun University of Science and Technology, Changchun* 130022, *China*

(Received 2 April 2020; revised manuscript received 19 June 2020; accepted manuscript online 1 August 2020)

We proposed a vanadium dioxide (VO_2)-integrated multi-functional metamaterial structure that consists of three metallic grating layers and two VO_2 films separated by SiO_2 dielectric spacers. The proposed structure can be flexibly switched among three states by adjusting temperature, incident direction, and polarization. In state 1, the incident wave is strongly transmitted and perfectly converted to its orthogonal polarization state. In state 2, the incident wave is perfectly absorbed. In state 3, incident wave is totally reflected back. The working frequency of the multi-functional metamaterial can be arbitrarily tuned within a broad pass band. We believe that our findings are beneficial in designing temperature-controlled metadevices.

Keywords: metamaterial, vanadium dioxide, multi-functionality

PACS: 42.79.Ci, 42.25.Ja, 78.20.Bh **DOI:** 10.1088/1674-1056/abab6f

1. Introduction

Recently, the optical properties of metamaterial have been widely studied in scientific community. Various metamaterials have been presented to achieve novel functions such as asymmetric transmission,[1–3] polarization conversion,[4,5] and perfect absorption.[6,7] In conventional metamaterials, metal is used in the structure construction, which usually results in great difficulties in dynamic control once fabricated. To overcome this issue, graphene,[8–16] Dirac semimetal,[17–21] and strontium titanate[22] are introduced in metamaterial design to achieve dynamic control via applying bias voltage, doping, and temperature. However, these works mainly concern about the control of working frequency or intensity of only one metamaterial function. Most recently, metamaterials that are integrated with phase change materials have been widely studied. Among the phase change materials, vanadium dioxide (VO_2) is more interesting because its reversible insulator–metal phase transition around the temperature of 340 K,[23] accompanied with structural variation from the monoclinic phase to the rutile phase VO_2 is particularly interesting because its reversible phase transition can be achieved through various external stimuli such as thermal heating,[24] applied current,[25] and optical pumping.[26] Song *et al.* proposed a VO_2-integrated metamaterial which can achieve the transition of absorption-electromagnetically induced transparency.[27] Ding *et al.* presented a VO_2-integrated metamaterial that realizes the switching between two functions of broadband absorption and reflecting broadband half-wave plate.[28] In these works, two functions switched by temperature are concerned. However metamaterials possessing two more switchable functions are seldom studied.

In this paper, we numerically investigate the multi-functionality of a VO_2-based terahertz metamaterial structure by using the finite-difference time-domain (FDTD) method. The proposed structure consists of three metallic grating layers and two VO_2 films separated by SiO_2 dielectric spacers. We first investigate the optical properties of the structure when VO_2 is at insulator phase. Simulation results show that two pass bands that possess perfect polarization conversion effect can be achieved when illuminated with *y*-polarized wave, while for *x*-polarization incidence the incident wave is reflected back over the whole interested pass band. Then we investigate the performance of the structure when VO_2 is at metal phase. The incident wave is totally absorbed for *y*-polarization incidence and reflected back for *x*-polarization incidence. Thus, three effects (state 1 transmitting with perfect polarization conversion, state 2 perfectly absorbing, and state 3 totally reflecting) are achieved. We optimize the geometric parameters to adjust the three effects to work at the same frequency, and finally acquire the multi-functional metamaterial that can be flexibly switched among three working states. Results also show that the working frequency of the multi-functional metamaterial can be arbitrarily tuned within a broad pass band by adjusting the geometric parameters of the structure.

*Project supported by the Scientific and Technological Developing Scheme of Jilin Province, China (Grant No. 20180101281JC), the "135" Research Project of Education Bureau of Jilin Province, China (Grant No. JJKH20190579KJ), and the "111" Project of China (Grant No. D17017).

†Corresponding author. E-mail: zjh@cust.edu.cn

© 2020 Chinese Physical Society and IOP Publishing Ltd

2. Structure design and simulation method

Figure 1 shows the schematic diagram of the proposed metamaterial. As shown in Fig. 1(a), the proposed metamaterial consists of three metallic layers and two VO_2 films separated by dielectric spacers. The three metallic layers are grating structures as shown in Figs. 1(b)–1(d). The grating ribbons of front and back layers are parallel to the x axis and the y axis, respectively. The grating ribbons of the middle layer are oriented at 45° with respect to the x axis. In the simulation, the metallic grating is made of gold with a conductivity of $\sigma = 4 \times 10^7$ S/m.[29] The dielectric spacers are chosen as SiO_2 with a refractive index of 1.95.[30] VO_2 is modeled as a phase change material, the conductivity of VO_2 at different temperatures can be acquired from Ref. [31]. Though the conductivity changes with frequency, it varies within a narrow range. Approximatively, we model its metal phase and insulator phase respectively by the conductivity of $\sigma = 2 \times 10^5$ S/m and the dielectric permittivity of 12 with a conductivity of $\sigma = 0$ S/m.[27] Thus, the phase change process of VO_2 can be simulated by switching between the two cases. The thicknesses of the metallic layers and the VO_2 films are 0.2 μm and 1 μm, respectively. In the original structure, the other parameters shown in Fig. 1 are $t_g = 5.5$ μm, $t_s = 57$ μm, $w_1 = 56$ μm, $g_1 = 14$ μm, $w_2 = 16$ μm, and $g_2 = 8.75$ μm. The proposed structure is possible to be fabricated by repeating deposition and transfer processes and the gold grating layers can be acquired by electric beam evaporation and conventional optical lithography.[29]

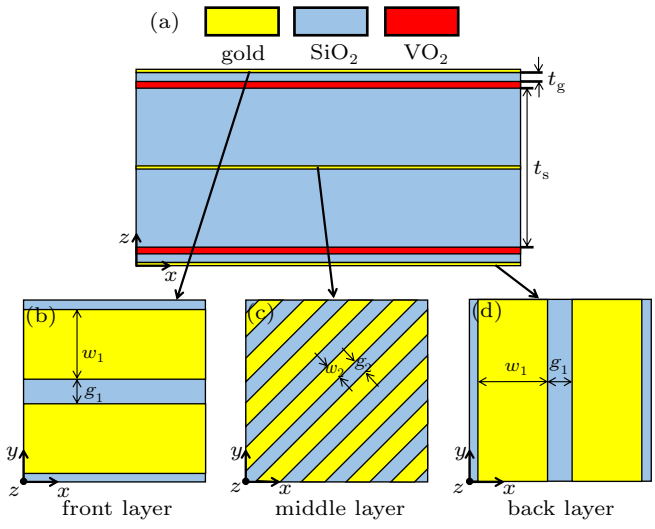


Fig. 1. (a) Cross section view of the proposed metamaterial. The thickness of the upper part is the same as that of the lower part. (b) Front, (c) middle, and (d) back metallic grating layers of the proposed metamaterial. The front grating is parallel to the x axis, the middle grating is oriented at 45° with respect to the x axis and the back grating is vertical to the x axis.

In the investigation of the optical properties of the structure, we performed the simulations by using the finite-difference time-domain (Lumerical FDTD solutions) method. In the simulations, the structure is placed in the air. Perfectly matched layer (PML) boundary conditions that absorb light waves with minimal reflections are applied in the $\pm z$ directions to mimic an infinite space. Periodic boundary conditions with a period of 70 μm are applied in the x and y directions. In the simulation, we show the results for forward propagation ($-z$ direction) only, because the forward propagated x- (y-) polarized wave meets the same structure as that of backward propagated y- (x-) polarized wave.[32]

3. Optical characteristics and the realization of multi-functionality

3.1. A switchable polarization convertor and perfect reflector when VO_2 is at insulator phase

When VO_2 is at insulator phase (298-K room temperature), the VO_2 film acts as a dielectric film that is transparent for THz wave.[28] For the originally proposed structure, the simulation results are shown in Fig. 2. Figure 2(a) shows the moduli $|T_{ij}|$ of the T matrix coefficients.[32]

$$\begin{pmatrix} t_x \\ t_y \end{pmatrix} = \begin{pmatrix} T_{xx} & T_{xy} \\ T_{yx} & T_{yy} \end{pmatrix} \begin{pmatrix} i_x \\ i_y \end{pmatrix} = T_{\text{lin}}^{\text{f}} \begin{pmatrix} i_x \\ i_y \end{pmatrix}, \tag{1}$$

where i and t represent the complex amplitudes of the incident and transmitted waves, the subscripts x and y represent the polarization directions, lin represents the linear polarization state, and the superscript f indicates the forward propagation (defined as the $-z$ direction in this work). We can see that there are two bands around the frequencies of 0.453 THz and 1.058 THz present high cross-polarization coefficient $|T_{xy}|$ and low co-polarization coefficient $|T_{yy}|$, which indicates strong transmission with polarization conversion effect for y-polarized incident wave. While the transmission coefficients $|T_{xx}|$ and $|T_{yx}|$ for x-polarization incidence are simultaneously low, indicating a blocking for x-polarized wave. Therefore, for y-polarization incidence, the incident wave is mostly transmitted when incident from the front side and the transmitted wave can be converted to its orthogonal polarization state (x-polarization). The conversion efficiency can be expressed as the polarization conversion ratio (PCR)

$$\text{PCR}_y = \frac{|T_{xy}|^2}{|T_{xy}|^2 + |T_{yy}|^2}. \tag{2}$$

The transmittance and PCR curves are shown in Fig. 2(b). We can see that the PCR shown by the red dashed curve is near unity in the whole interested band, indicating a perfect polarization conversion effect. The total transmission is shown by the black solid curve in Fig. 2(b) which shows two working

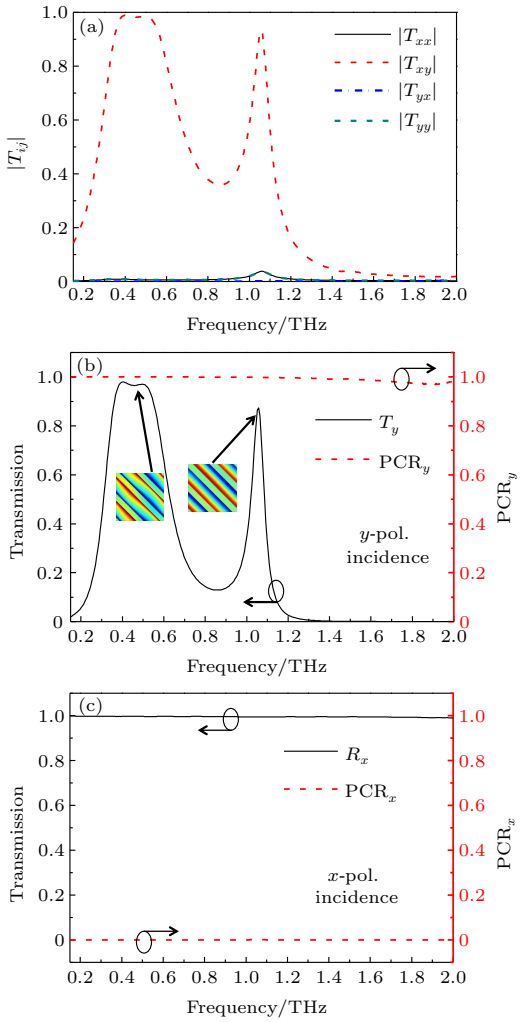


Fig. 2. (a) Moduli of the T matrix coefficients for forward propagation. (b) Transmission and PCR spectra for y-polarization (y-pol.) incidence. Insets are z-component electric field distributions in the middle x–y plane of the middle grating structure at the frequencies of 0.453 THz and 1.058 THz, respectively. (c) Reflection and PCR spectra for x-polarization (x-pol.) incidence.

pass bands of high transmittance for perfect polarization conversion effect around 0.453 THz and 1.058 THz. The insets in Fig. 2(b) show the z-component electric field distributions obtained from the surface of the middle metallic grating at 0.453 THz and 1.058 THz, respectively. The two kinds of electric field distributions indicate different transmitting modes at the two working frequencies. For x-polarization incidence, as analyzed above, the incident wave is mostly blocked. We show, in Fig. 2(c), the reflectance by the black solid curve, from which we can see that the incident wave is perfectly reflected back (by the metallic grating[33]). We also show the PCR, by the red dashed curve in Fig. 2(c), for the reflected wave calculated based on the reflection matrix[5] (not shown here). There is no polarization conversion effect for x-polarization incidence. Therefore, when VO_2 is at insulator phase, y-polarized incident wave along $-z$ direction can be converted to x-polarized wave in two pass bands, while x-polarized incident wave can be totally reflected back without polarization conversion.

3.2. A switchable perfect absorber and reflector when VO_2 is at metal phase

When VO_2 is at metal phase (378 K), the VO_2 films act as two reflection mirrors, along with the metallic grating structures on both sides of the metamaterial, two metal–insulator–metal (MIM) structures are generated, which are usually designed to perfectly absorb light incident from the air side. Figure 3(a) shows the absorption spectra for y-polarized incident wave when incident from front side. We can see that a resonance absorption peak locates at the frequency of 1.155 THz

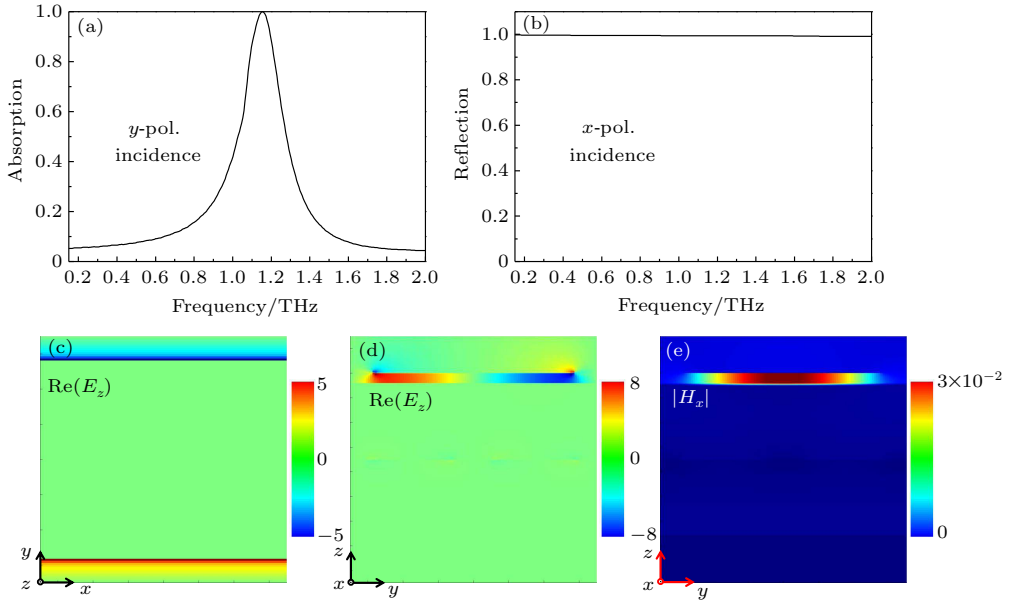


Fig. 3. (a) Absorption spectrum for y-polarization incidence. (b) Reflection spectrum for x-polarization incidence. (c) The z-component electric field distribution in the x–y plane of the front grating layer, (d) the z-component electric field distribution in the y–z plane of the structure, and (e) the magnetic $|H_x|$ field distribution in the y–z plane at the frequency of 1.155 THz when illuminated with y-polarized wave.

with an absorptivity of 99.9%. While for x-polarization incidence, as shown in Fig. 3(b), the incident wave is also totally reflected back (by the metallic grating[33]). We present, in Figs. 3(c)–3(e), the field distributions of y-polarization incidence for forward propagation to reveal the absorption mechanism. Figures 3(c) and 3(d) show the z-component electric field distributions at the resonance frequency of 1.155 THz. It is obvious that a dipole resonance parallel to the y axis is excited on the metallic grating structure. The electric dipole is strongly coupled with the metal phased VO_2 film, resulting a magnetic polariton that induces a strong magnetic resonance as shown in Fig. 3(e). Then, in the proposed structure, perfect absorption can be achieved.[34]

4. Optimization for the multi-functionality of the metamaterial

For y polarization, when VO_2 is at metal phase, the absorption intensity of the structure is mainly determined by the dielectric layer thickness t_g[35] as shown in Fig. 4(a). We can see that the absorption peak value first rises then descends when t_g changes from 4.5 μm to 7.5 μm, and $t_g = 5.5$ μm is the optimal parameter for near perfect absorption at the frequency of 1.155 THz. Thus, we keep the thickness $t_g = 5.5$ μm unchanged in the optimization process. Then we optimize the parameters of the metamaterial to ensure that the metal-phased absorption and insulator-phased transmission work at the same frequency.

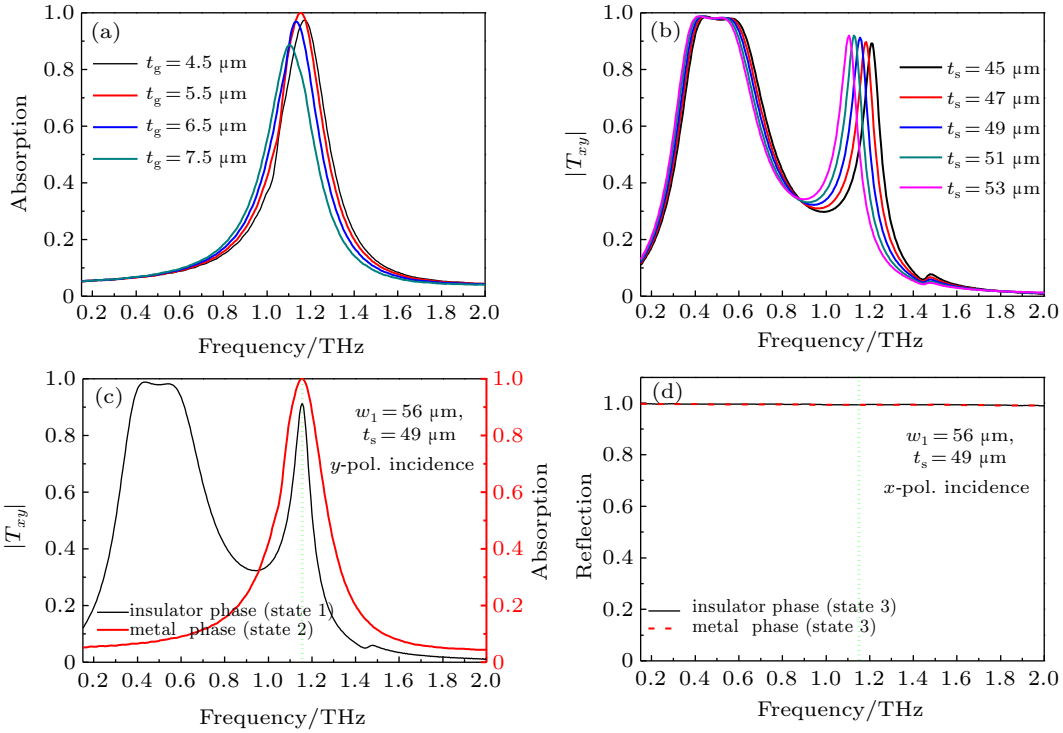


Fig. 4. (a) The absorption spectra with different t_g when VO_2 is at metal phase, and (b) the cross-polarization coefficient $|T_{xy}|$ with different t_s when VO_2 is at insulator phase for y-polarization incidence. (c) The absorption spectrum at metal phase and the cross-polarization coefficient at insulator phase for the optimized structure with $w_1 = 56$ μm, $t_s = 49$ μm when illuminated with y-polarized wave. (d) The reflection spectra of the optimized structure with $w_1 = 56$ μm, $t_s = 49$ μm at metal phase and insulator phase when illuminated with x-polarization wave.

Generally, the MIM absorption structure is independent of the middle dielectric spacer due to the segregation of the metal-phased VO_2 film, *i.e.*, the thickness of the middle dielectric spacer t_s has no impact on the reflection effect of the MIM structure. Figure 4(b) shows the cross-polarization coefficients $|T_{xy}|$ for forward propagation at insulator phase with different values of t_s, from which we can see that the polarization spectrum undergoes a redshift as t_s increases. Thus, in Fig. 4(b), we shift the mode located at the higher frequency of the insulator phase to match the perfect absorption frequency (1.155 THz) of the metal phase by adjusting t_s to 49 μm from the original designed structure (keeping $t_g = 5.5$ μm). As a result, we plot, in Fig. 4(c), the cross-polarization coefficient $|T_{xy}|$ and absorption spectrum for insulator and metal phases, respectively. Obviously, at the frequency of 1.155 THz, the optimized metamaterial can be flexibly switched between two states by changing the phase of VO_2 via temperature change. In state 1, y-polarized wave is strongly transmitted and perfectly converted to x-polarized wave. In state 2, y-polarized wave is perfectly absorbed. Moreover, for x-polarization incidence as shown in Fig. 4(d), whatever the phase of VO_2 is, the incident wave is totally reflected back by the front metallic grating, which is defined as state 3.

Next we investigate the alterable working frequency of the multi-functional metamaterial. According to the LC circuit model, the working frequency of the absorber can be derived by[35]

$$f_m = \frac{1}{2\pi\sqrt{LC/2}} \sim \frac{1}{w_1\sqrt{\varepsilon_d}}, \tag{3}$$

with w_1, L, C, and ε_d being the metallic grating width, the inductance, the capacitance, and the dielectric constant of dielectric layer. We can get the conclusion that the working frequency of the absorber is inversely proportional to the value of w_1. We simulate the absorption spectra of the structure for different values of w_1 with the period of the grating $P = 70$ μm remaining unchanged. The simulation results are shown in Fig. 5(a). When the grating width increases from 42 μm to 68 μm, the dipole moment is lengthened, resulting in redshift of the absorption peak, which agrees well with the theoretical analysis. In addition, a much wider or narrower grating will shift the dipole resonance out of the Fabry–Perot resonance band, resulting in the weakening of the Fabry–Perot enhanced absorption. Thus, the working frequency of the metal-phased perfect absorption can be arbitrarily tuned within a specified pass band by changing the grating width. And we can also adjust the middle dielectric spacer thickness t_s to achieve the multi-functionality at each specific working frequency following the steps illustrated above.

Taking the structure with $w_1 = 62$ μm for example. The working frequency of the metal-phased absorption is 1.035 THz as shown in Fig. 5(a). In Fig. 5(b), we shift the mode located at the higher frequency at insulator phase by tuning the middle spacer thickness t_s (from the structure with $w_1 = 62$ μm) to match the perfect absorption frequency of the metal phase. When the middle spacer thickness $t_s = 56$ μm, the peak frequency possessing strong transmission with perfect polarization conversion reaches also 1.035 THz, which agrees well with the perfect absorption frequency of the metal phase, as shown in Figs. 5(c). We also present the reflection spectra for x-polarization incidence at insulator and metal phases in Fig. 5(d). The total reflection effects can be achieved at both the phases of VO_2 film. Based on Figs. 5(c) and 5(d) we can conclude that another multi-functional metamaterial with the working frequency of 1.035 THz is achieved.

Therefore, by adjusting geometric parameters, the working frequency of the multi-functional metamaterial can be arbitrarily tuned within a broad pass band. At the working frequencies, three states (state 1 transmitting with perfect polarization conversion, state 2 perfectly absorbing, and state 3 totally reflecting) can be flexibly achieved by adjusting the conditions of polarization state and temperature. Moreover, all results presented above are acquired through forward propagation, however due to the symmetric property of the proposed metamaterial, an exactly opposite result can be acquired for backward propagation. The specific conditions corresponding to each state are listed in Table 1.

Table 1. The corresponding conditionsfor the three states.

	Conditions for state 1	Conditions for state 2	Conditions for state 3
Forward propagation	y-pol. and 298 K	y-pol. and 378 K	x-pol.
Backward propagation	x-pol. and 298 K	x-pol. and 378 K	y-pol.

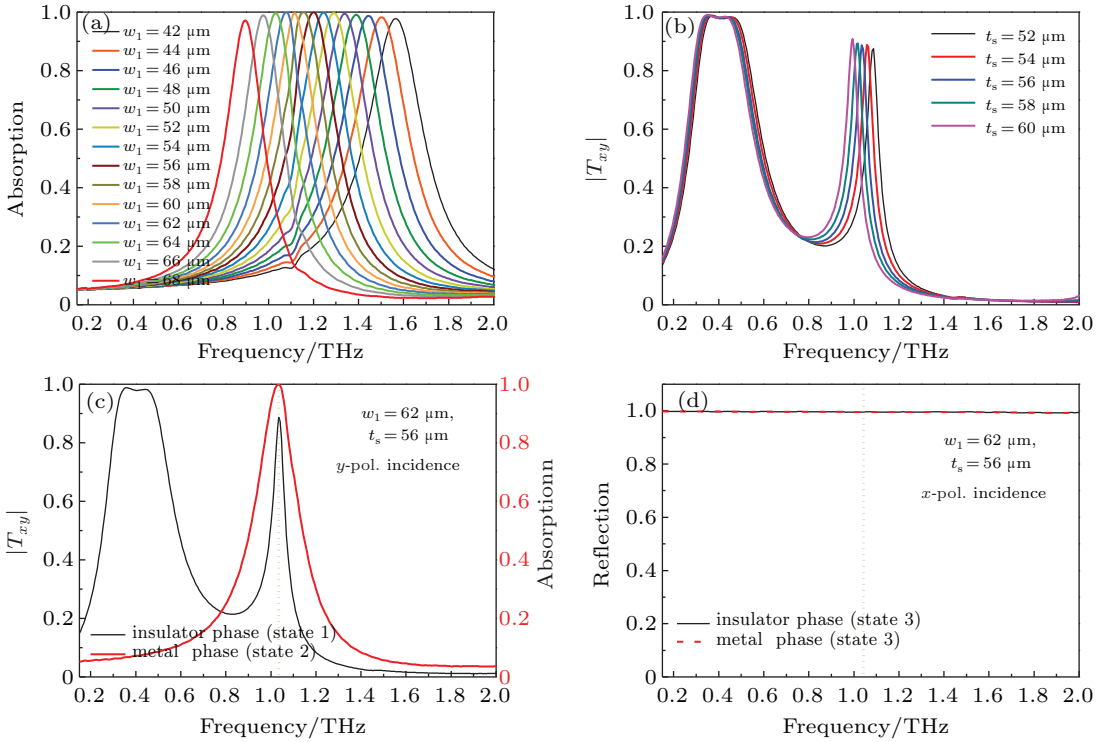


Fig. 5. (a) The absorption spectra with different w_1 when VO_2 is at metal phase, and (b) the cross-polarization coefficient $|T_{xy}|$ with different t_s when VO_2 is at insulator phase for y-polarization incidence. (c) The absorption spectrum at metal phase and the cross-polarization coefficient at insulator phase for the optimized structure with $w_1 = 62$ μm, $t_s = 56$ μm when illuminated with y-polarized wave. (d) The reflection spectra of the optimized structure with $w_1 = 62$ μm, $t_s = 56$ μm at metal phase and insulator phase when illuminated with x-polarization wave.

5. Conclusion

In summary, we have proposed a VO_2-integrated metamaterial structure that can be flexibly switched among three states by adjusting temperature, incident direction, and polarization. The metamaterial consists of three metallic grating layers and two VO_2 films separated by SiO_2 dielectric spacers. FDTD simulations show that the proposed structure can be flexibly switched among three working states. In state 1, the incident wave is strongly transmitted and perfectly converted to its orthogonal polarization state. In state 2, the incident wave is perfectly absorbed. In state 3, incident wave is totally reflected back. The working frequency of the multi-functional metamaterial can be arbitrarily tuned within a broad pass band.

References

[1] Menzel C, Helgert C, Rockstuhl C, Kley E B, Tunnermann A, Pertsch T and Lederer F 2010 *Phys. Rev. Lett.* **104** 253902
[2] Shi J, Liu X, Yu, S, Lv, T, Zhu, Z, Ma H and Cui T 2013 *Appl. Phys. Lett.* **102** 191905
[3] Zhao J, Fu Y, Liu Z and Zhou 2017 *Opt. Express* **25** 23051
[4] Floess D, Chin J Y, Kawatani A, Dregely D, Habermeier H, Weiss T and Giessen H 2015 *Light: Sci. Appl.* **4** e284
[5] Yang C, Luo Y, Guo Y, Pu Y, He D, Jiang Y, Xu J and liu Z 2016 *Opt. Express* **24** 16913
[6] Yao G, Ling F, Yue J, Luo C, Ji J and Yao J 2016 *Opt. Express* **24** 1518
[7] Luo J and Lin Y 2019 *Appl. Phys. Lett.* **114** 051601
[8] Zhu L, Liu F, Lin H, Hu J, Yu Z, Wang X and Fan S 2016 *Light: Sci. Appl.* **5** e16052
[9] Guo T and Argyropoulos C 2016 *Opt. Lett.* **41** 5592
[10] Rodrigo D, Tittl A, Limaj O, Abajo F J C, Pruneri V and Altug H 2017 *Light: Sci. Appl.* **6** e16277
[11] He X, Liu F, Lin F and Shi W 2019 *Opt. Express* **27** 13831
[12] He X, Lin F, Liu F and Zhang H 2019 *Nanomaterials* **10** 39
[13] Zhao Y, Wu B, Huang B and Cheng Q 2017 *Opt. Express* **25** 7161
[14] Huang X, He W, Yang F, Ran J, Gao B and Zhang W 2018 *Opt. Express* **26** 25558
[15] Zeng B, Huang Z, Singh A, Yao Y, Azad A K, Mohite A D, Taylor A J, Smith D R and Chen H 2018 *Light: Sci. Appl.* **7** 51
[16] Huang Y, Yao Z, Hu F, Liu C, Yu L, Jin Y and Xu X 2017 *Carbon* **119** 305
[17] Liu G, Zhai X, Meng H, Lin Q, Huang Y, Zhao C and Wang L 2018 *Opt. Express* **26** 11471
[18] Zhao J, Song J, Zhou Y, Zhao R and Zhou J 2019 *IEEE Photonics J.* **11** 4601709
[19] Meng H, Shang X, Xue X, Tang K, Xia S, Zhai X, Liu Z, Chen J, Li H and Wang L 2019 *Opt. Express* **27** 31062
[20] Luo J, Lin Q, Wang L, Xia S, Meng H and Zhai X 2019 *Opt. Express* **27** 20165
[21] Dai L, Zhang Y, O'Hara J F and Zhang H 2019 *Opt. Express* **27** 35784
[22] He X, Lin F, Liu F and Shi W 2020 *J. Phys. D: Appl. Phys.* **53** 155105
[23] Morin F J 1959 *Phys. Rev. Lett.* **3** 34
[24] Kim B J, Lee Y W, Chae B G, Yun S J, Oh S Y, Kim H T and Lim Y S 2007 *Appl. Phys. Lett.* **90** 023515
[25] Fan L, Chen Y, Liu Q, Chen S, Zhu L, Meng Q, Wang B, Zhang Q, Ren H and Zou C 2016 *ACS Appl. Mater. Interfaces* **8** 32971
[26] Guo P, Weimer M S, Emery J D, Diroll B T, Chen X, Hock A S, Chang R P H, Martinson A B F and Schaller R D 2017 *ACS Nano* **11** 693
[27] Song Z, Chen A, Zhang J and Wang J 2019 *Opt. Express* **27** 25196
[28] Ding F, Zhong S and Bozhevolnyi S I 2018 *Adv. Opt. Mater.* **6** 1701204
[29] Zhang Y, Feng Y, Jiang T, Cao J, Zhao J and Zhu B 2018 *Carbon* **133** 170
[30] Naftaly M and Miles R E 2007 *J. Appl. Phys.* **102** 043517
[31] Cai H, Chen S, Zou C, Huang Q, Liu Y, Hu X, Fu Z, Zhao Y, He H and Lu Y 2018 *Adv. Opt. Mater.* **6** 1800257
[32] Huang C, Feng Y, Zhao J, Wang Z and Jiang T 2012 *Phys. Rev. B* **85** 195131
[33] Zhao J, Song J, Xu T, Yang T and Zhou J 2019 *Opt. Express* **27** 9773
[34] Liu Y, Zhong R, Huang J, Lv Y, Han C and Liu S 2019 *Opt. Express* **27** 7393
[35] Wang B, Zhai X, Wang G, Huang W and Wang L 2015 *Opt. Mater. Express* **5** 227